Inhibition and Thermodynamics of *Escherichia coli* Peptide Deformylase

Undergraduate Thesis

Presented in partial fulfillment of the requirements
for graduation *with distinction*
from The Ohio State University

Amber Simmons

*****

The Ohio State University
Winter 2007

Dissertation Committee:

Professor Mark P. Foster, Advisor

Professor Venkat Gopalan

Professor Terry Gustafson

Approved by

_____

College of Biological Sciences

ABSTRACT

Peptide deformylase (PDF) is a bacterial metalloenzyme responsible for cleaving the formyl group from nascent polypeptides, aiding in their maturation. Because it is essential for the survival of bacterial cells and does not appear to play a necessary role in humans, PDF is an attractive antibacterial target. Actinonin is a naturally occurring compound that acts as a substrate analog to bind PDF and inhibit the enzyme's activity, therefore providing a potential template for developing new antibiotics. Described here are various dynamic features of PDF and the PDF-actinonin complex and thermodynamic properties of the binding event of actinonin to PDF.

Isothermal titration calorimetry (ITC) experiments were performed to provide thermodynamic information (K_A, ΔG, ΔH, and ΔS) about the binding of actinonin to PDF. First, because the identity of the bound divalent metal affects the catalytic activities of PDF, the thermodynamics of actinonin binding to Ni-, Co-, and Zn-PDF were explored. The association constant (K_A) was found to be highest for Zn-PDF and similar for the Ni- and Co-bond protein. These data also showed a correlation between the efficiency of catalysis (k_{cat}/K_M) and the thermodynamics (ΔH, ΔS) of actinonin binding. To assess the degree to which changes in protein motions contribute to binding, the change in heat capacity (ΔC_p) between the free and bound state was determined by measuring the temperature dependence of the enthalpy change, ΔH, upon binding. The effects of salt concentration and buffer on the ΔH were assessed to control for binding-linked processes that could contribute to the measured change in heat capacity. The value of ΔC_p, -177.5 $^{cal}/_{mol \cdot K}$, is larger in magnitude than the value expected from changes in molecular surface hydration, consistent with the hypothesis that changes in molecular motion do contribute to the thermodynamics of actinonin binding.

To characterize the effect of actinonin binding on the stability and motions in PDF, hydrogen-deuterium (H/D) exchange experiments using nuclear magnetic resonance (NMR) spectroscopy were performed on both free and actinonin-bound PDF. The binding of actinonin resulted in a large increase in protection of amide bonds in the binding pocket of PDF and entropically favored decreases of protection of amide bonds on the opposite side of the protein. These results are consistent with previous relaxation data.

Dedicated to Mom and Dad

TABLE OF CONTENTS

LIST OF TABLES

LIST OF FIGURES

Chapter 1: Introduction

Importance of novel antibiotics

Antibiotic resistance is a growing complication in the treatment of bacterial infections. The widespread prescription of antibiotics and their misuse in the last fifty years has led the emergence of antibiotic resistant bacteria, limiting the usefulness of many classes of antibiotics. In fact, about 70% of bacteria that cause infection in hospitals are resistant at least one type of antibiotic (1) and over 1,000 people die each year due to various strains methicillin-resistant *Staphylococcus aureus* (MRSA) (2). Another particularly threatening bacterium, multi-drug resistant *Mycobacterium tuberculosis* (MDR-TB) is resistant to the most potent antibiotics that are available and is currently running rampant in overcrowded Russian prisons (3). It is only a matter of time until this strain infiltrates large cities everywhere on the globe. Therefore, it is urgent that scientists, physicians, and clinicians develop new antibiotics to overcome this problem.

Today bacteria are developing antibacterial resistances faster than scientists can develop new treatments. To avoid a potential pandemic, scientists need to expedite current methods of drug discovery and development. The traditional method for novel drug discovery is a random screening method, which involves screening microbes from countless soil samples in hopes of finding naturally occurring antibiotics. This method, although it has advantages, is very time- and labor-intensive and has various limitations (4). Another method currently used to develop new drugs is to slightly alter already available drugs to reinitiate their effectiveness. This method, however, is also limited in that the new compound will often have a smaller bacterial spectrum for which it is useful and different classes of antibiotics will not likely be discovered. Structure-based drug design is a third method of drug discovery and development that has recently been gaining popularity. In structure-based drug design of antibiotics, one incorporates the knowledge of the structure and dynamics of a bacterial protein into the design a new ligand, made from scratch, which will interact with the protein and change its activity. Bacterial enzymes are promising molecules to investigate because their active sites constitute a binding site to which a specific ligand can bind. An analog of the natural substrate can make an effective

drug. A large and often difficult requirement for design of a novel drug is a complete characterization of the factors that govern binding.

The binding of two molecules is regulated by the thermodynamics of the binding event, in particular, the overall change in free energy accompanying binding. The change in free energy is defined as:

$$\Delta G = \Delta H - T\Delta S$$

where ΔG is the change in Gibbs free energy, ΔH is the change in enthalpy, T is temperature, and ΔS is the change in entropy. Change in heat and energy can contribute to ΔH, as well as the change in exposed surface area or a molecule. ΔS is essentially a measure of "disorder". Conformational entropy, rotational/translational entropy, and the hydrophobic effect can all contribute to ΔS. Structural and dynamical properties of the system can help elucidate these parameters. For example, S^2 values can be obtained through ModelFree analysis from which ΔS values can be calculated. It is these thermodynamic parameters that must be defined for a comprehensive understanding of the mobility of the drug target, which in turn will facilitate drug development. (5, 6)

Peptide Deformylase

Protein synthesis in all prokaryotes is initiated by an *N*-formylmethionine residue. Maturation of a vast majority of the proteins includes the removal of the *N*-formyl moiety, a step that is often necessary to generate a functional protein. This cleavage is performed by peptide deformylase (PDF). Roughly 50% of proteins also require a second step in maturation, the removal of the N-terminal methionine residue which is undertaken by methionine amino peptidase (MAP). MAP cannot perform its peptidase activity with the *N*-formyl group still on the methionine (7).

Although eukaryotic cells do not initiate their peptide synthesis with an *N*-formylated methionine and do not require PDF for maturation, a gene homologous to the one for PDF in bacteria is present in the genome of eukaryotic mitochondria and chloroplasts (8). This homology was not obvious at first because the overall sequence is not highly conserved among prokaryotic and eukaryotic nuclear PDF, but the three-dimensional structures are surprisingly conserved. Modest differences in the substrate binding pocket of *Arabidopsis thaliana* and

bacterial PDF suggest that specificity could be incorporated into a new antibacterial drug. The tertiary structure of a human nuclear PDF will aid in this understanding (9).

E. coli peptide deformylase (PDF) has proven to be an excellent model to study dynamics and ligand binding for novel drugs. PDF is highly conserved in the kingdom of Bacteria and is essential for them to thrive. *E. coli* peptide deformylase is a 19.2 kDa protein consisting of 168 amino acids. Residues 1-147 compose the catalytic core while the last 21 residues form a C-terminal α-helix that is not essential for activity and is not present in other organisms such as *Streptococcus pyogenes*, *Streptococcus pneumonia*, and *Clostridium beijerinckii* (10). The *E. coli* PDF structure includes a divalent cation coordinated in a tetrahedral arrangement with two histidine residues, His^{132} and His^{136}, a cysteine residue, Cys^{90}, and a water molecule. The two histidine residues are present in a conserved HEΦDH motif and the cysteine residue is the middle of a conserved EGCΦS motif, where Φ is any hydrophobic amino acid (7) (figure 1.1). Another highly conserved GΦGΦAAxQ motif lies adjacent to the binding pocket, where *x* is any amino acid. The divalent cation to which PDF is complexed is a ferrous ion *in vivo* (11). This form of PDF, however, is difficult to work with in the laboratory because the ferrous ion oxidizes to a ferric ion upon exposure to air. Zinc, nickel, and cobalt are practical substitutes and do not significantly change the structure of PDF (12, 13, 14, 15). The structures of PDF from several organisms in the presence of various metals and inhibitors have been solved by x-ray crystallography and NMR spectroscopy (11, 16-27). These structures show that PDF consists of three α-helices, three 3_{10} helices, and seven β-strands which create three anti-parallel β-sheets. The residues present in PDF's active site are highly conserved.

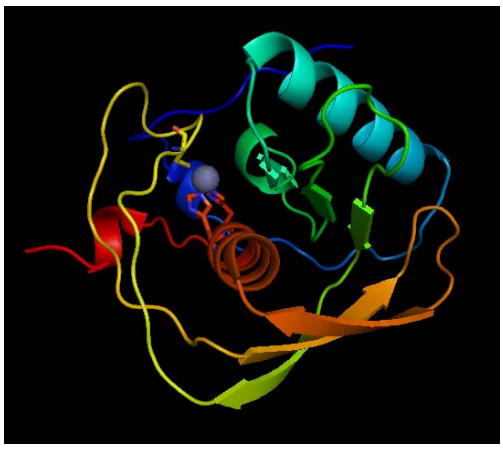

Figure 1.1 Backbone cartoon diagram of *E. coli* Zn-PDF. Cys^{90}, His^{132}, and His^{136} are shown as sticks. The active site metal ion (Zn^{2+}) is shown as a purple sphere, PDB ID: 1BS5

The structure of PDF is homologous to a family of zinc metalloproteases that are present in humans and responsible for tissue repair. Human enzymes in this family include thermolysin, stromelysin, and angiotenisin-converting enzyme (14, 28). Activities of these enzymes are vital in avoiding pathological conditions such as arthritis, multiple sclerosis, and hypertension (29, 30). The similarities between PDF and this zinc metalloprotease family create the challenge of

developing a drug specific enough to eliminate PDF activity and allow the activities of the human enzymes to remain uninhibited. Comprehensive investigation of ligand binding in PDF is essential to circumvent this caveat.

It is not a question of "if" bacterial resistance to PDF-targeting drugs will emerge, but "when". It is possible for bacteria to become resistant to a PDF inhibitor by eliminating the initial formylation of the N-terminal methionine residue, an action performed by methionyl-$tRNA^{fMet}$ formyltransformylase. It has been shown that these mutants are not as healthy as wild-type bacteria, but can still flourish (9).

Actinonin as a drug template

Actinonin is a naturally occurring PDF inhibitor that was isolated in 1960 from *Streptomyces* and identified as a potential antibiotic (mechanism unknown) via random screening techniques (figure 1.2 a.) (31). Peptide deformylase was not even identified until 8 years later and in 2000 it was recognized that actinonin inhibits PDF (15, 31). Actinonin inhibits PDF *in vitro*, displays tight binding with a K_i value (where 50% of the protein is inhibited) of 0.3 nM and demonstrates bacteriostatic activity against a wide range of Gram-positive and Gram-negative bacteria. The inhibition mechanism involves binding of a hydroxamate group on the inhibitor to the metal ion of PDF. Actinonin itself is toxic to human cells because it inhibits other amino peptidases such as seminal alanyl aminopeptidase (15). Importantly, only the hydroxamate group on the chemical structure of the inhibitor is essential for antibacterial activity; the rest of the molecule can be altered.

BB-3497 is a molecule derived from actinonin that has a K_i of 7 nM and, unlike actinonin, it is orally bioavailable (Figure 1.2 b.) (32). Excitingly, it was shown in mice that BB-3497 is effective against a methicillin resistant strain of *S.*

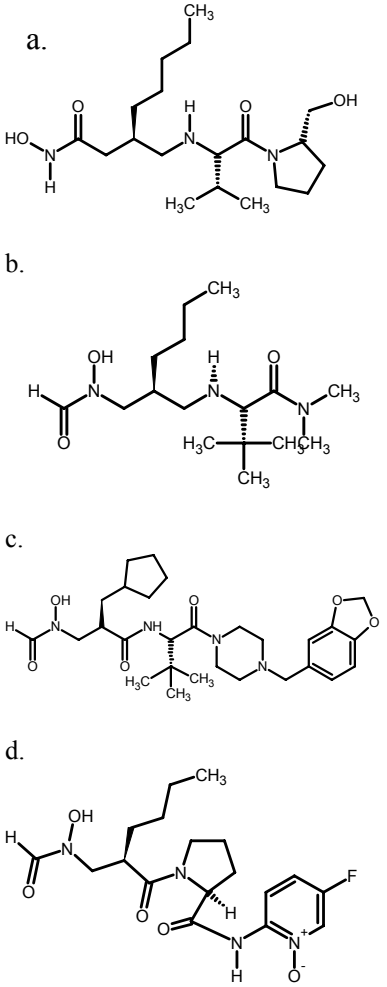

Figure 1.2 a. Actinonin (15), b. BB-3497 (32), c. BB-83698 (32), d. LBM415 (34)

aureus! BB-83698 is another actinonin derivative which became the first PDF inhibitor to advance to phase one clinical trials in 2004 (Figure 1.2 c.) (7, 33). One year later another PDF inhibitor, LBM415, progressed to clinical trials (Figure 1.2 d.) (34).

Isothermal Titration Calorimetry

To explore the nature of the PDF-actinonin binding event isothermal titration calorimetry (ITC) experiments were performed. ITC can directly measure the change of enthalpy, ΔH, associated with the binding reaction and the binding constant, K_A, can be calculated by fitting the binding curve. In ITC, one binding partner is placed in a cell and the calorimeter measures exactly how much power needs to be put into the cell to maintain a fixed temperature. Small injections of the other binding partner are infused into the cell and, as the binding event takes place, heat will be either released or absorbed by the reaction depending on whether the event is exothermic or endothermic. A thermogram of power (µcal/sec) vs. time (min) is generated where the spikes represent the power surge following each injection (Figure 1.3 a.). An isotherm is constructed by plotting the area under each spike vs. the molar ratio of titrant to analyte, which is calculated by the starting concentrations of each species (Figure 1.3 b.). The isotherm (plot of areas) can be fit to an equation with which one can deduce ΔH, which is essentially the difference between the maximum binding energy released/absorbed and the baseline. The thermodynamic quantities that were measured with ITC, K_A and ΔH, can be used to calculate the change in free energy, ΔG, and the change in entropy, ΔS, using fundamental thermodynamic relationships:

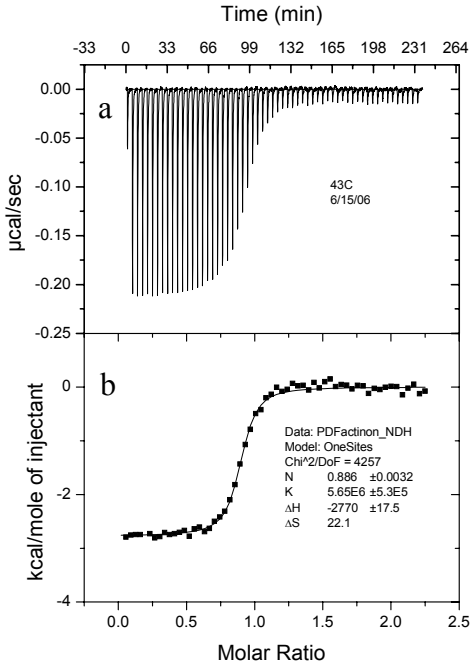

Figure 1.3. a. An ITC isotherm, b. an ITC thermogram.

$$\Delta G = -RT\ln(K_A)$$

and $$\Delta G = \Delta H - T\Delta S.$$

Despite similarities between the crystal structures of PDF containing zinc, cobalt, nickel, and iron, it has been shown that the zinc chelated peptide deformylase (Zn-PDF) has a much lower efficiency of catalysis than the iron (Fe-PDF, the natural form of PDF), cobalt (Co-PDF), or nickel (Ni-PDF) forms (14, 35). It has also been shown that the binding of actinonin to Zn-PDF is tighter than that of Fe-PDF, Ni-PDF, or Co-PDF, suggesting that Zn-PDF may bind the substrate too tightly for the enzyme to accomplish its function. The data gathered from ITC will help explain these phenomena.

Two ITC experiments were performed earlier by a former graduate student in the Foster Laboratory: an actinonin/Zn-PDF binding titration at 27°C and one at 37°C. Only one run per set of conditions was performed and only five or six data points defined the transition regions of the curves, which is used to calculate K_A. These experiments were repeated to better define the K_A.

Hydrogen/Deuterium Exchange Using Nuclear Magnetic Spectroscopy

By comparing the crystal structures of free and actinonin-bound PDF it has been suggested that there is a loss of internal motion within PDF when it binds to actinonin (5) and, therefore, a loss of conformational entropy. However, this appears to be offset by a gain in entropy from the hydrophobic effect, or the release of water molecules upon burial of non-polar surface area. Since the binding event is driven by a large favorable change in entropy as determined by previous, preliminary ITC experiments, the change in the dynamics of side-chain residues were thought to play an important role in ligand binding. Hydrogen/deuterium exchange experiments that provide residue-specific thermodynamic information were undertaken to corroborate this idea.

To compare the thermodynamics of specific residues in free PDF and actinonin-bound PDF, hydrogen/deuterium exchange experiments were preformed using NMR. NMR is a powerful technique that can be used to probe physical, chemical, and structural information about a molecule. There are many ways of utilizing NMR; in this project, two-dimensional ^{1}H-^{15}N Heteronuclear Single Quantum Coherence (HSQC) spectra were used. An HSQC spectrum shows a signal for every ^{1}H-^{15}N bond in the molecule so, for a protein uniformly labeled with ^{15}N, there should be one peak for every residue except for proline, which contains a secondary

nitrogen (and no ^{1}H), plus peaks from amino acid side chains with N-H bonds, such as asparagine.

When a protein is in solution, the amide protons that are exposed to solvent will exchange freely with the protons in the solvent. The rate of exchange of protons provides direct information about the accessibility of the proton to solvent and, consequently, the fold of the protein. A protein made with ^{1}H can be submerged in a deuterated aqueous solution- D_2O ($^{2}H_2O$). The amide protons will exchange with the deuterons is solution and, since a bond between an ^{15}N and a D will not produce a signal in the ^{1}H-^{15}N HSQC, the rate of exchange can be obtained from the rate at which the signal disappears.

In folded proteins, nitrogen-bound protons constantly equilibrate between "open" and "closed" states that correspond to unfolded and folded states. Only when an amide group is in the open state can the proton be exchanged with a deuteron from the solution.

$$NH(closed) \xleftrightarrow{K_{op}} NH(open) \xrightarrow{k_{ch}} exchanged$$

Amide protons can be protected from exchange if they are involved in secondary structures, such as an alpha-helix, or buried deep inside the protein. For exchange rates to be observed for protected amides, small-scale local unfolding events must take place often involving breakage of hydrogen bonds for access to the solvent (36). Under normal conditions, the proton exchange rate, k_{ex}, is given by equilibrium constant, K_{op}, multiplied by the exchange rate in the open state, k_{ch}:

$$k_{ex} = K_{op} k_{ch.}$$

The Gibbs free energy of a closed amide is associated with a value G_c, as is the free energy of the open state, G_o. The difference between the two states is the change in free energy, ΔG. The free energy associated with each amide can be correlated with the exchange data and represented mathematically as:

$$\Delta G = -RT\ln(K_{op}) = -RT\ln(k_{ex}/k_{ch}),$$

where R is the ideal gas constant, 1.987 $^{cal}/_{mol \cdot K}$, T is the temperature, and K_{op}, k_{ex}, and k_{ch} are as previously defined.

By measuring the rate of hydrogen atom exchange for all amides in both free PDF and actinonin-bound PDF, how binding of actinonin alters the thermodynamics of each residue in the protein can be quantified. These data can be combined with other dynamic data gathered from

relaxation experiments and data calculated from changes in the free and actinonin-bound PDF crystal structures to convey exactly what is occurring in the actinonin-PDF binding event.

Chapter 2: Expression and Purification of *E. coli* Peptide Deformylase

The expression and purification protocol for PDF was adapted from the protocol in D.W. Byerly's Ph.D. thesis (5). *E. coli* BL21(DE3) cells were transformed with pET-22b-def (encoding PDF residues 1-147) using either heat shock or electroporation. Unlabeled Zn-PDF cells were grown in Luria-Bertani broth; ^{15}N-labeled cells, Co-PDF, and Ni-PDF were grown in M9 minimal media with 10 mL Eagle basal vitamin mix (Life Technologies) per liter, both media supplemented with 50 μg/L carbenicillin. Cells were incubated in a shaker at 37°C and once the culture reached an OD_{600} of 0.6-0.8, cells were induced by adding 1 mM IPTG. At this time 100 μM $ZnCl_2$, $CoCl_2$, or $NiSO_4$ was added to the medium, depending on the desired cation to be chelated to PDF. The culture was incubated overnight (~18 h). In the morning, the cells were harvested by centrifugation for 30 min at 30,000 g in a Sorvall SS-34 rotor. The cell pellet was resuspended in 30 mL buffer A (20 mM TRIS, pH 8.0, 10 mL NaCl) with 100 μg/mL PMSF (Boeringer Manheim) and sonicated for 2 x 5 min with 2 sec pulses. The solution was centrifuged at 30,000 g for 30 min. The soluble lysate was filtered and loaded onto a 35-mL Q Sepharose fast flow column (Pharmacia) previously equilibrated with buffer A. Protein was eluted from the column with a 200 mL linear salt gradient from 10 mM to 1 M NaCl (figures 2.1, 2.2). The fractions that included PDF, as indicated on a SDS-PAGE gel, were purified using gel filtration column in buffer C (20 mM TRIS, pH 6.8, 10 mM NaCl) at 3 mL/min. Fractions containing PDF were combined and concentrated by ultrafiltration (Centriprep-10, Americon). SDS-PAGE gel showed that the protein was purified to near homogeneity (figure 2.3).

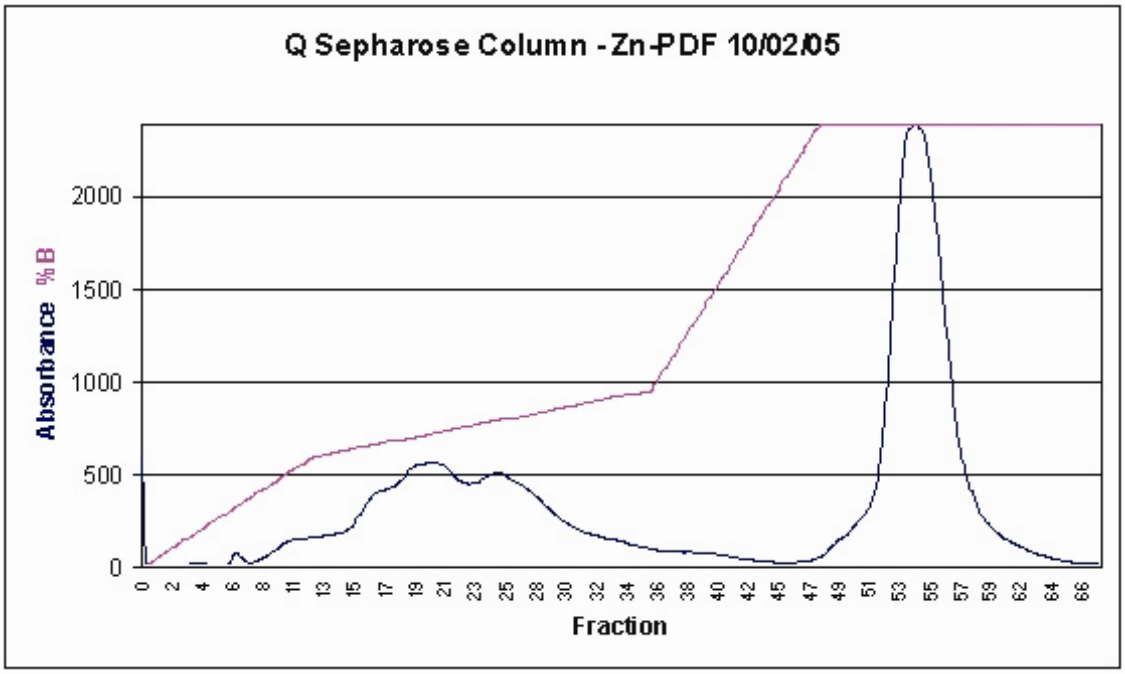

Fig. 2.1 Chromatogram of protein elution from Q Sepharose column. PDF eluted between fractions 23 and 30.

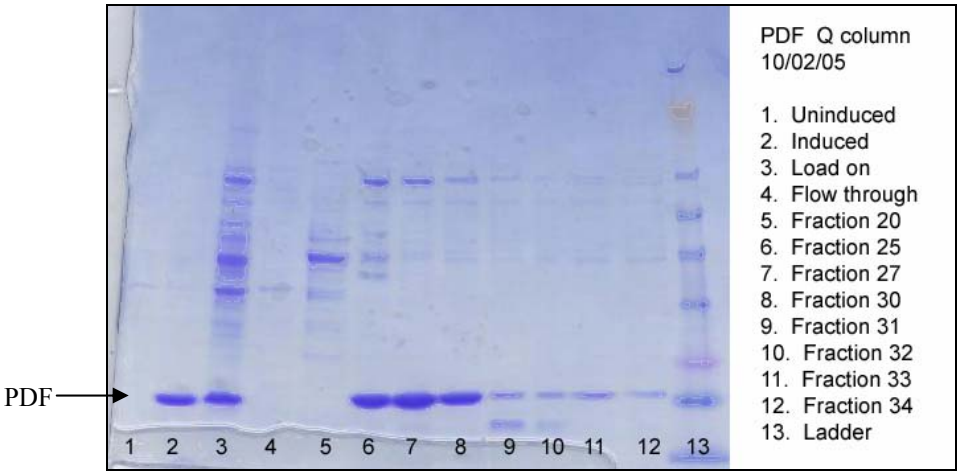

Figure 2.2 SDS-PAGE gel of PDF purification from induction to Sepharose Q column.

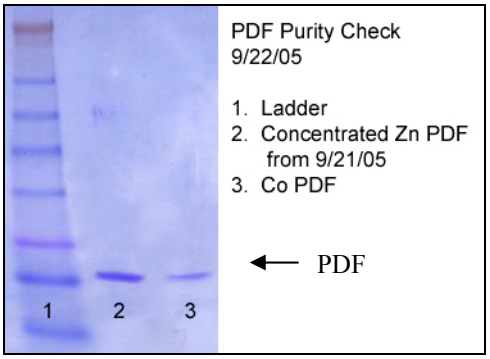

Figure 2.3 SDS-PAGE gel showing homogeneity of PDF after final step of purification.

Chapter 3: Isothermal Titration Calorimetry

Introduction

Isothermal titration calorimetry (ITC) was utilized to explore the thermodynamics of PDF binding to actinonin. ITC offers direct measurements the change in enthalpy, ΔH, and data from which the binding constant, K_A, can be calculated. From these quantities, ΔG and ΔS can be calculated. Because of the temperature dependence of ΔH, experiments at different temperatures permit the calculation of heat capacity, ΔC_p (37). All thermograms are shown in the appendix.

Calculation of Heat Capacity

The ΔC_p of actinonin binding to PDF was found by performing actinonin-PDF binding experiments at different temperatures. Experiments were performed between 13°C and 43°C at 6°C intervals. To determine ΔC_p, data were taken from the experiments performed at 13°C, 19°C, 37°C, and 43°C; the experiments performed at 25°C and 31°C did not provide crisp transitions between unsaturated and saturated enzymes because it is in this range where ΔH is near zero and binding is driven by ΔS. The data were plotted and fit to a linear equation:

$$\Delta H = \Delta C_p (T - T_h)$$

where T = temperature at which the experiment was performed and T_h = the temperature at which the binding enthalpy is zero (38). The plot is shown below:

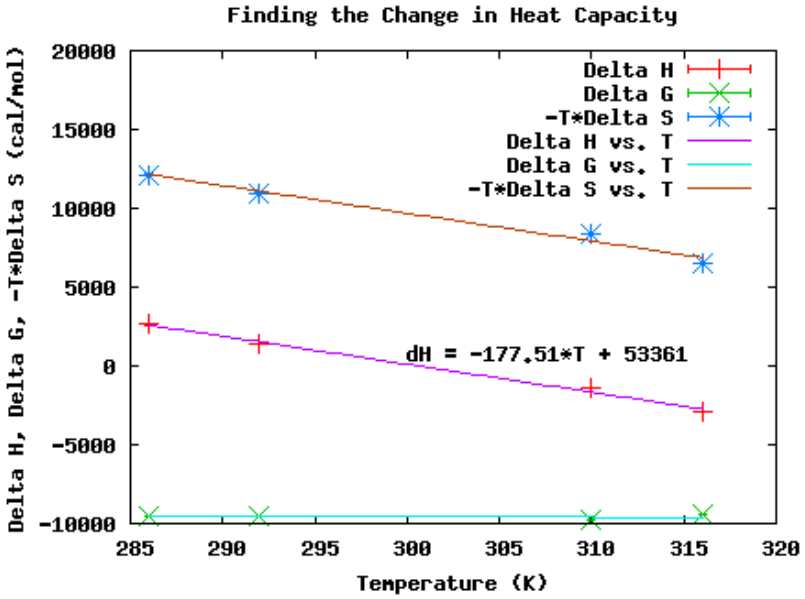

Table 3.1 The effect of temperature on thermodynamic properties of PDF-actinonin binding.

ΔG was calculated with the equation $\Delta G = -RT\ln(K_A)$ and $T\Delta S$ was calculated by subtracting the calculated ΔG from the measured ΔH. The change in heat capacity (ΔC_p) is defined by $\delta\Delta H/T$; therefore, the slope of a line drawn through the data points on a plot of ΔH vs. temperature defines ΔC_p. ΔC_p was calculated to be -177.5 $^{cal}/_{mol\cdot K}$. The value of the measured ΔC_p is larger than the value expected solely from changes in molecular surface area (-80.8 $^{cal}/_{mol\cdot K}$) (5). Factors that could contribute to this difference are: salt bridge formation, proton uptake, burial of interfacial water and/or changes in molecular motions (dynamics) (39, 40). The burial of interfacial water molecules would be observable when comparing the crystal structures of PDF free and complexed with actinonin. No water molecules appear to be buried in the PDF-actinonin complex crystal structure. To explore the possibilities of salt bridge formation and proton uptake, further ITC experiments were performed.

Testing for Ion Linkage

One can determine if ion linkage is taking place by performing ITC experiments in solvents with various salt concentrations. Actinonin was titrated into Zn-PDF in TRIS buffer with 10 mM NaCl, 150 mM NaCl, and 300 mM NaCl. If the rearrangement of atoms in PDF caused the formation or disruption of a salt bridge, the binding affinity (K_A) of the reaction would increase as the salt concentration increases due to stronger electrostatic interactions and plot of $\log(K_A)$ vs. log[NaCl] would exhibit a linear relationship (39). The results of these experiments are shown below.

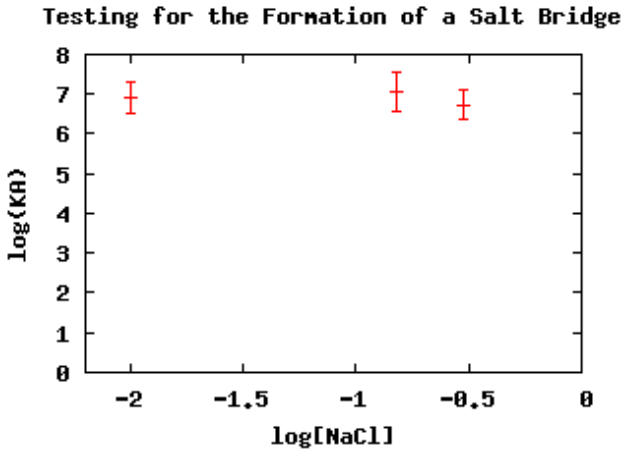

Table 3.2 The effect of salt on PDF-actinonin binding.

No correlation between salt concentration and binding affinity is apparent, implying that a salt bridge does not form upon the binding of actinonin to PDF.

Testing for Proton Linkage

If proton linkage occurs upon ligand binding, it can be observed by performing calorimetry experiments at different pHs. However, because pH may change the shape of the protein, experiments were performed in different buffers with different heats of ionization. If a proton uptake from the buffer occurs upon actinonin binding, the change in enthalpy for the binding event in different buffers would be drastically different- at least upon an order of magnitude (40). ITC experiments were performed with tris(hydroxymethyl)aminomethane (TRIS), 4-(2-hydroxyethyl)-1-piperazineethanesulfonic acid (HEPES), and cacodylic acid buffers. Results are shown below.

Buffer	Heat of Ionization (kcal/mol) (ref 42)	K_A (cal/mol)	Delta H (cal/mol)
TRIS	-11.340822	8.25E6 ± 3.4E6	-1416 ± 23.6
HEPES	-4.875717	4.23E6 ± 4.8E5	-1444 ± 14.7
Cacodylic Acid	-0.7170172	9.98E6 ± 8.3E6	-1204 ± 46.7

Table 3.3 ITC in different buffers, testing for proton linkage.

Since the change in enthalpy is insignificant across this range of heat of ionization values, a proton uptake does not appear to occur when PDF and actinonin bind.

Comparing Thermodynamic Properties of PDF Complexed with Different Divalent Cations

The crystal structures of PDF containing iron (the natural metal), cobalt, nickel, and zinc are all similar, but they each have different catalytic activities. Although Zn-PDF is the least active, it binds actinonin the strongest. ITC experiments were performed with Zn-PDF, Co-PDF, and Ni-PDF to determine if thermodynamic properties of the actinonin-binding reactions could help explain this phenomenon. ITC experiments for Fe-PDF were not attempted because of the readiness of Fe^{2+} to oxidize upon exposure to air. The results are summarized in Table 3.4.

The metals are listed in the order of highest catalytically activity first and the least active last. With the highest K_A value, Zn-PDF binds the ligand the strongest. These data suggest that perhaps Zn-PDF binds the substrate too tightly for efficient catalysis to take place. In addition,

Metal	Cation Size (g/mol)	k_{cat}/K_M (ref 14 & 34)	K_A (M)	ΔH (cal/mol)	ΔG (cal/mol)	-TΔS (cal/mol)
Iron	55.85	3.50E+06				
Cobalt	58.93	1.11E+06	8.35E6 ± 1.94E6	-5079 ± 67.9	-9817 ± 0.22	-4738 ± 67.9
Nickel	58.69	5.38E+05	6.04E6 ± 2.78E6	-1891 ± 52.3	-9618 ± 0.45	-7727 ± 52.3
Zinc	65.39	3.10E+04	8.25E6 ± 3.42E6	-1416 ± 23.6	-9809 ± 0.28	-8394 ± 23.6

Table 3.4 Thermodynamic properties of PDF with different divalent cations, T = 37°C.

the binding of actinonin to Zn-PDF and Ni-PDF is driven primarily by favorable entropic changes while the binding of the ligand to Co-PDF is driven by enthalpic and entropic changes. It does not appear that the cation size, at least within this range, correlates strongly with catalytic efficiency or thermodynamic properties.

Methods

PDF was expressed and purified as discussed in Chapter 2. The protein was concentrated to between 32 and 40 μM, as measured by absorbance. The protein was dialyzed overnight and the dialysate was used to dilute the actinonin sample from 25 mM to exactly 10x that of the protein. Both samples were degassed thoroughly.

ITC measurements were performed using a MicroCal VP-ITC instrument. The protein solution in the cell was stirred at 300 rpm by the syringe to ensure rapid mixing. 59- 5 μM injections of actinonin were made into the cell containing PDF with 240 sec between each injection. Data were analyzed using Origin V.7 SR4 MicroCal. The baseline and the beginning and end of each peak were adjusted manually. The last few points of the titration, after the solution was saturated, were averaged and subtracted from each data point to correct for heat of dilution. Origin uses a non-linear, method of least squares via minimization of χ^2 and the concentrations of the titrant and the analyte to fit the energy flow per injection to an equilibrium binding equation, supplying best fit values of the stoichiometry (n), change in enthalpy (ΔH), and the binding constant (K_A) (43).

Chapter 4: Hydrogen/Deuterium Exchange

Hydrogen/deuterium exchange experiments were performed to compare residue-specific thermodynamic effects of actinonin binding to PDF. Amide protons in the protein that are exposed to solvent will exchange freely with protons in the solvent. Hydrogen bonding, other electrostatic interactions, and tertiary structure in macromolecules impede this exchange process, thus slowing the rate of exchange. However, local unfolding events enable protected protons to exchange with the solvent (44).

Results and Discussion

PDF was diluted to a 90% D_2O solution and immediately subjected to NMR. HSQCs were taken at least every hour for 24 hours. The intensities of each peak was measured and plotted as a function of time. The data were then fit to an exponential curve:

$$y = A0*exp(-A1*x)+A2$$

where *A0* = the y-intercept, *A1* = the rate, and *A2* = the offset. The N-H pairs that exchanged their protons within the first 15 minutes exchanged too fast for measurement of an accurate rate, since it took about 15 min to acquire the first HSQC. There were also some that did not exchange even after 24 h. Peak assignments were completed by Doug Byerly and Craig McElroy from the Foster Laboratory. An overlay of seven HSQCs over various time points is shown in figure 4.1. Representative plots of residues displaying nice fits are shown in figure 4.2.

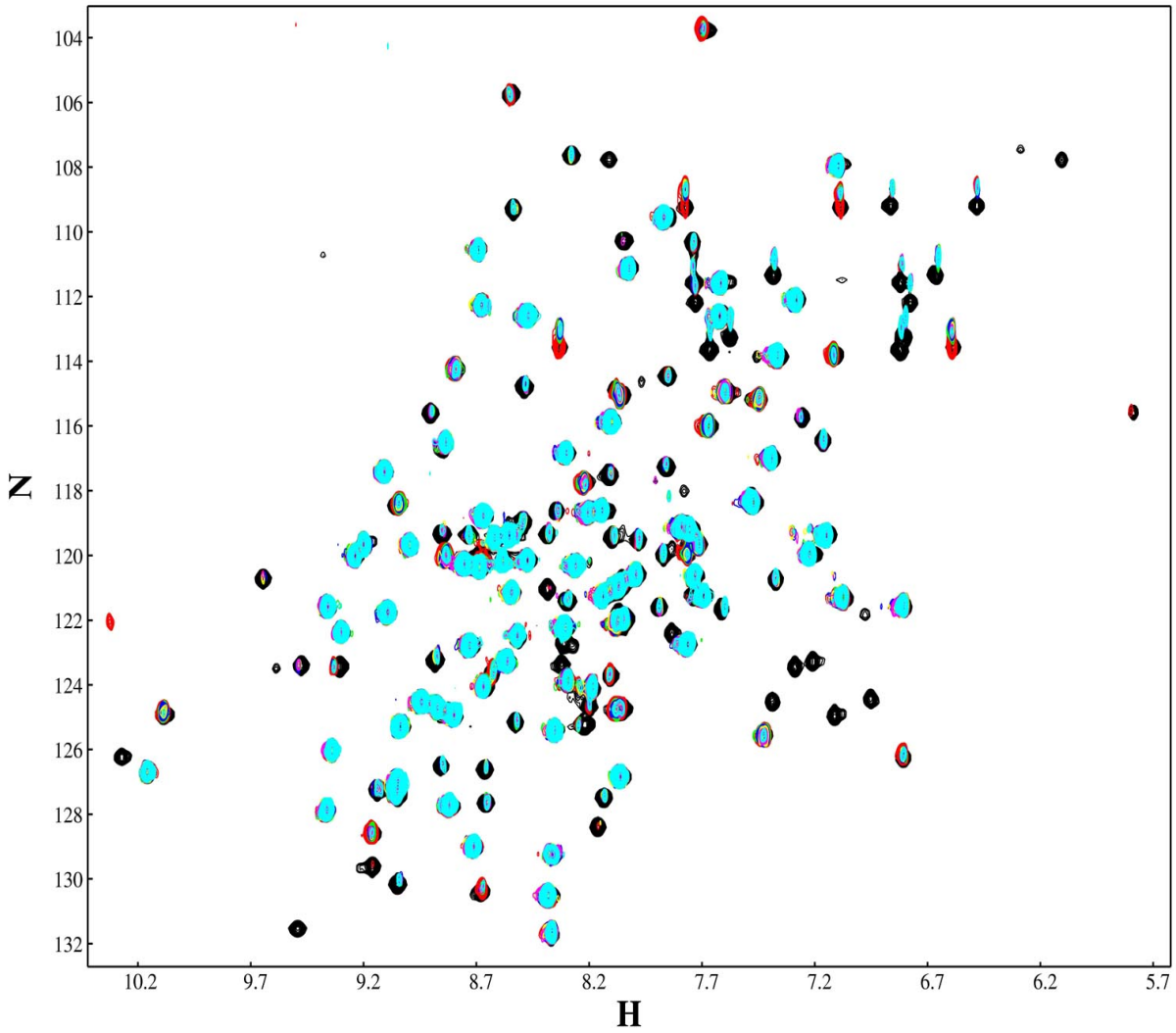

Figure 4.1 An overlay of seven HSQCs for the free PDF hydrogen-deuterium exchange experiment: **T=0 min, T=17, T=72, T=128, T=240, T=351, T=597 min.**

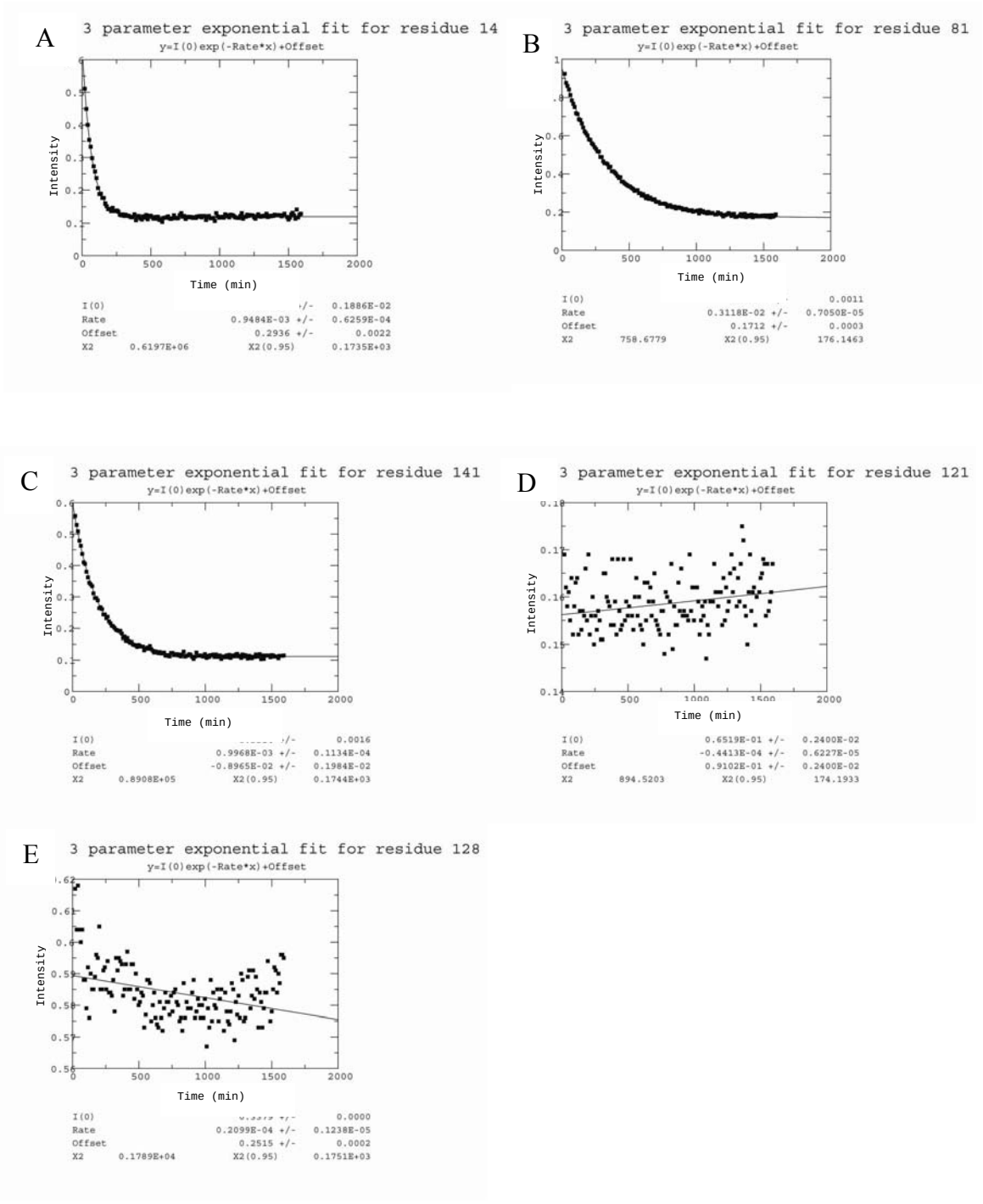

Figure 4.2 A, B, and C display regressions with good fits. D displays an amide that exchanged too fast for a rate to be measured. E did not exchange within 24 hours.

Exchange experiments show that there are large areas of both free PDF and actinonin-bound PDF that are completely protected from solvent and do not exchange even after 24 hours as well as regions that are exposed to solvent and exchange protons faster than on the minute-hour time scale. Rates for 35 residues were measured for free PDF and rates for 44 residues were measured for actinonin-bound PDF. Figure 4.3 shows the measured rates mapped to the structure of PDF.

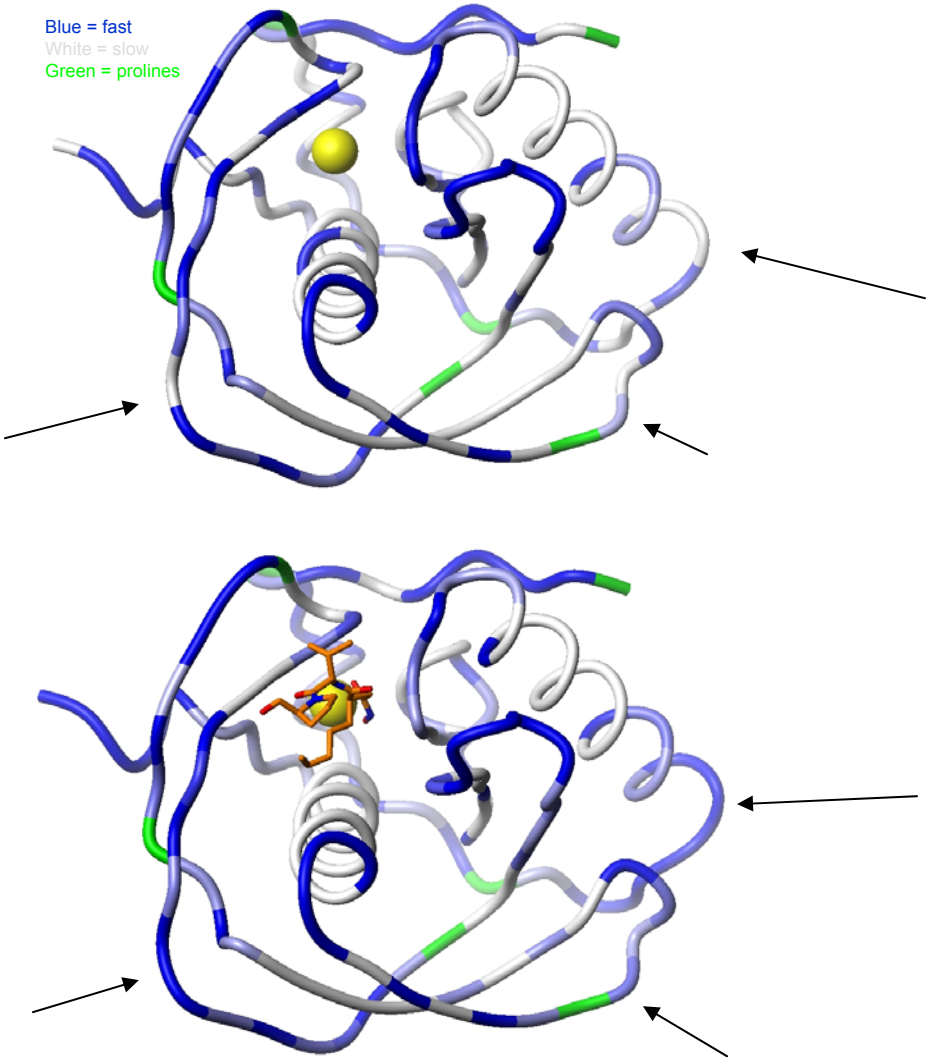

Figure 4.3 The top cartoon shows PDF free; actinonin-bound PDF is on the bottom. There is a gradient color scheme from white to blue, white indicating slow rate of exchange, blue illustrating fast rate of exchange. Prolines are shown in green, they do not have amide bonds. Actinonin is orange and the zinc atom is yellow. Arrows indicate regions that are more dynamic in the actinonin bound molecule than in the free PDF molecule.

Notice that neither the amide bonds within alpha helices nor the residues involved in beta-sheets exchange within 24 h. Also, the residues around the binding pocket of PDF become "lighter" (more white) upon the binding of PDF. These changes were expected. Many residues on the distal side of the protein, however, became more dynamic with the binding of actinonin. The regions are particularly apparent are labeled with arrows in Figure 4.3. The increase in flexibility on the region of the protein opposite of the active site offers entropic compensation for the decrease of mobility near the binding site. This is consistent with relaxation data collected previously (5).

The differences in the rates for each residue were assessed. Since the k_{ex} values are those of an exponential decay, to compare the rates directly the following equation was used:

$$Difference\ in\ rate = -\frac{1}{\log(k_{ex})_{free}} - \left(-\frac{1}{\log(k_{ex})_{bound}}\right)$$

The results are shown below:

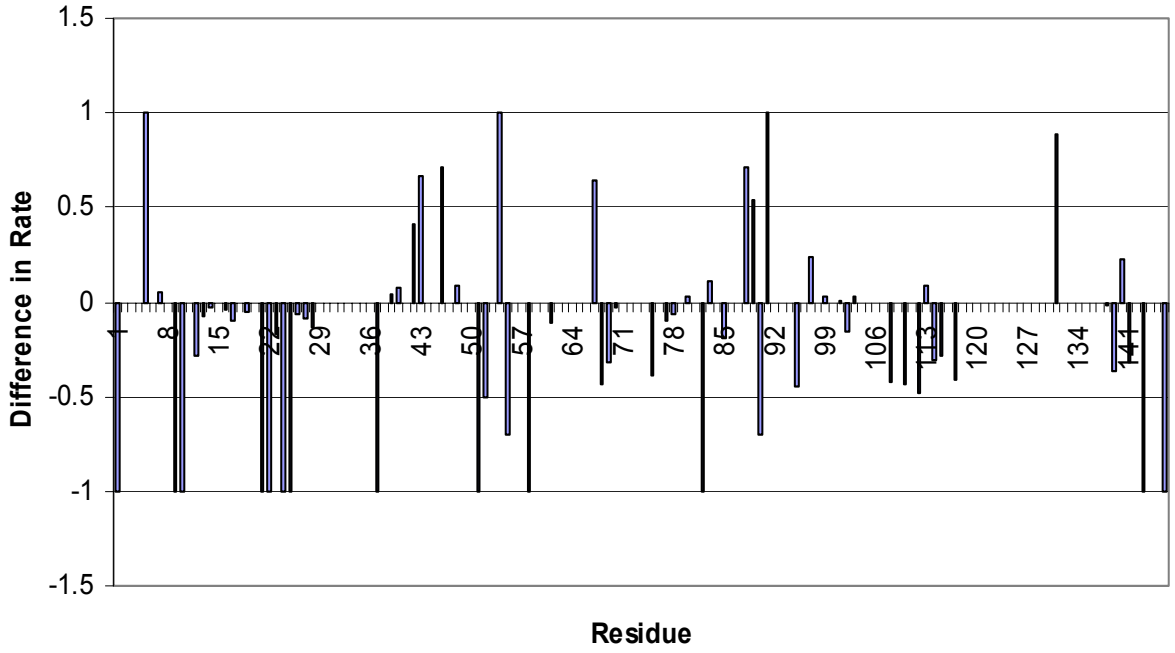

Figure 4.4 Differences in proton exchange rates between free and actinonin-bound PDF.

Protection factors are defined as the rate of proton exchange when the amide is in the fully solvent-exposed state to the rate of exchange when it is not fully solvent-exposed (36, 45):

$$P = \frac{k_{\text{int}}}{k_{ex}}$$

where k_{int} = the intrinsic exchange rate of the amide proton for that residue (these have been tabulated for each individual amino acid as a function of temperature and pH) and k_{ex} = the observed rate of exchange (36). Therefore, the protection factor is always greater than or equal to 1. By measuring the difference in protection factors between free and bounds states, one can determine the degree to which the exposure of solvent has changed and, therefore, any changes in structure and/or flexibility within a certain region of the protein. Because the rates trace exponential curves, the logarithm is taken to directly compare the values.

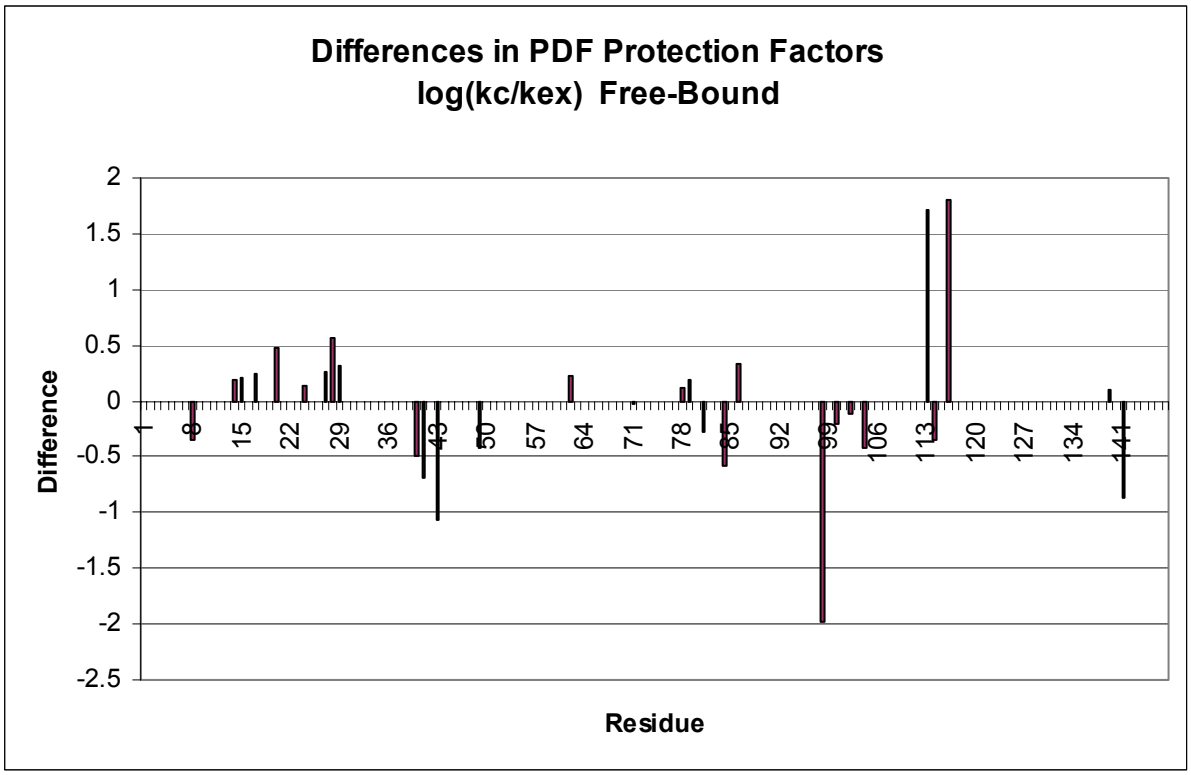

Figure 4.5 Differences in amide protection factors between free- and actinonin-bound PDF.

Residues 16-25 and 111-117 compose random coils on side of the protein opposite from the binding site. As the positive differences in protection factor implies, these are residues that, in general, are losing protection from solvent when the ligand binds. Their increase in dynamics most likely contributes to this loss of protection. Whereas residues 87-99 compose a random coil in the free PDF structure, hydrogen bonding between actinonin and Gly[89] and other electrostatic

interactions allow the formation of a beta-sheet in this region (15). The hydrogen bond that forms between Ala^{98} and Glu^{88} upon actinonin binding explains the large gain of protection for the amide in residue 98. Electrostatic interactions occur between actinonin and residues in the region of Ile^{44} and cause the gain of protection in that region.

Methods

^{15}N-labeled Zn-PDF was expressed and purified as described in chapter 2. 10% D_2O and 1% DSS in D_2O were added and the protein was concentrated to approximately 2 mM. For actinonin-bound samples, actinonin was added so that there was 0.1 mM excess to ensure that all PDF was bound. An HSQC was also taken to ensure complete binding of actinonin to PDF. Immediately before collecting data, the protein was diluted to a buffer containing 90% D_2O. The first HSQC spectrum was collected as soon as possible after the dilution, which was approximately 15 minutes because the sample needed to be aligned and the spectrometer tuned, matched, shimmed, and prepared to take data. Spectra were taken at least every hour for 24 hours. Data was collected on the Bruker DRX 800 MHz spectrometer at 310 K. All spectra were processed using NMRPipe and analyzed with NMRview. Intensities of peaks were fit to an exponential decay with CurveFit and analyzed using xmgrace.

Conclusions and Future Directions

Isothermal titration calorimetry (ITC) experiments were performed to provide thermodynamic information (K_A, ΔG, ΔH, and ΔS) about the binding of actinonin to PDF. To assess the degree to which changes in protein motions contribute to binding, the change in heat capacity (ΔC_p) between the free and bound state was determined by measuring the temperature dependence of the enthalpy change, ΔH, upon binding. The value of ΔC_p, -177.5 $^{cal}/_{mol \cdot K}$, is larger in magnitude than the value expected from changes in molecular surface hydration. The effects of salt concentration and buffer on the ΔH were assessed and it was found that these binding-linked processes do not contribute to the measured change in heat capacity. Therefore, it is changes in molecular motion do contribute to the thermodynamics of actinonin binding.

To assess the degree to which the divalent cation affects binding, actinonin was bound to Ni-, Co-, and Zn-PDF. The association constant (K_A) was found to be highest for Zn-PDF and similar for the Ni- and Co-bond protein. Because the efficiency of catalysis (k_{cat}/K_M) is lowest for Zn-PDF, it is thought that Zn-PDF binds the substrate too tightly for optimum rate of catalysis. The binding of actinonin to Zn-PDF and Ni-PDF is driven primarily by favorable entropic changes while the binding of the ligand to Co-PDF is driven enthalpic forces.

According to hydrogen-deuterium (H/D) exchange experiments, the binding of actinonin results in a large increase in protection of amide bonds in the binding pocket of PDF and entropically favored decreases of protection of amide bonds on the opposite side of the protein. These results are consistent with previous relaxation data.

The next phase of my peptide deformylase analysis will include molecular dynamic (MD) simulations. MD simulations are theoretical computer simulations that allow one to place a molecule in a virtual environment and allow it to interact under the known laws of physics. Using statistical mechanics, the molecule adopts allowed conformations in a certain amount of time and, therefore, allows for the study of the dynamics of a molecule.

APPENDIX A

ITC Thermograms

Different temperatures

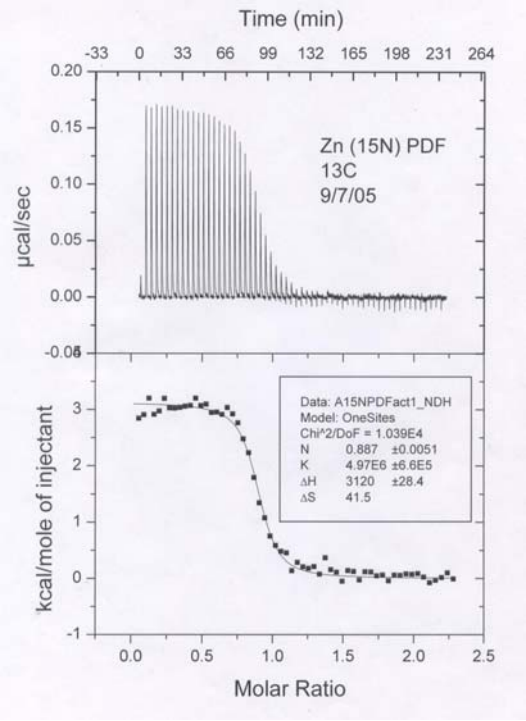

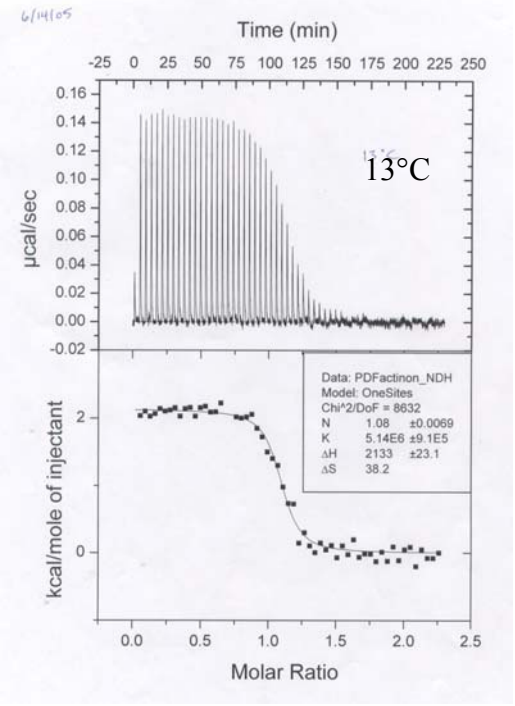

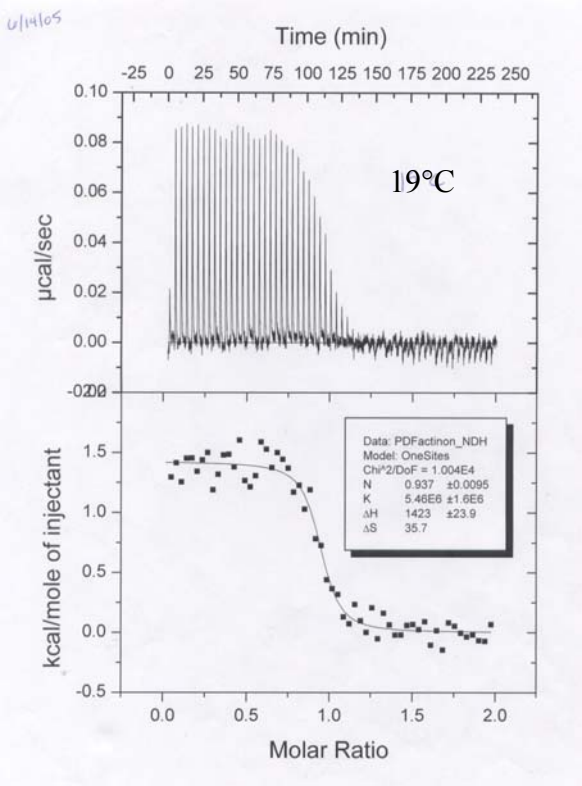
Time (min)
19°C
µcal/sec
kcal/mole of injectant
Molar Ratio
Data: PDFactinon_NDH
Model: OneSites
Chi^2/DoF = 1.004E4
N 0.937 ±0.0095
K 5.46E6 ±1.6E6
ΔH 1423 ±23.9
ΔS 35.7

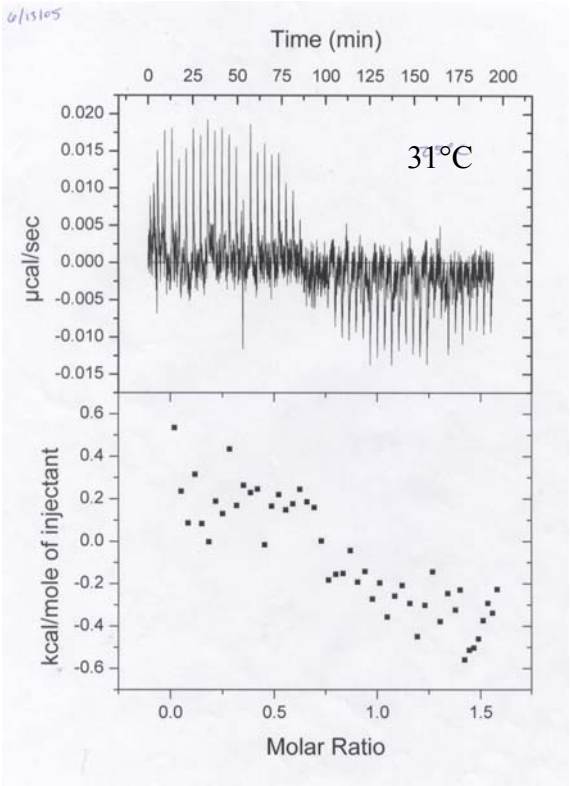
Time (min)
31°C
µcal/sec
kcal/mole of injectant
Molar Ratio

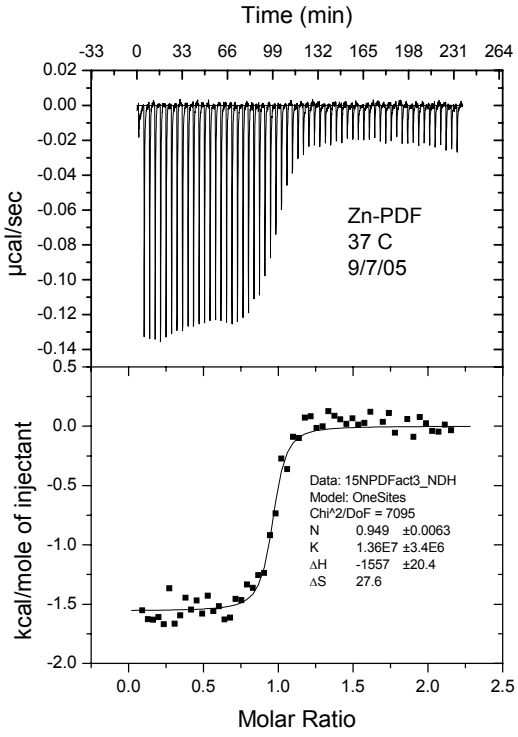
Time (min)
Zn-PDF
37 C
9/7/05
µcal/sec
kcal/mole of injectant
Molar Ratio
Data: 15NPDFact3_NDH
Model: OneSites
Chi^2/DoF = 7095
N 0.949 ±0.0063
K 1.36E7 ±3.4E6
ΔH -1557 ±20.4
ΔS 27.6

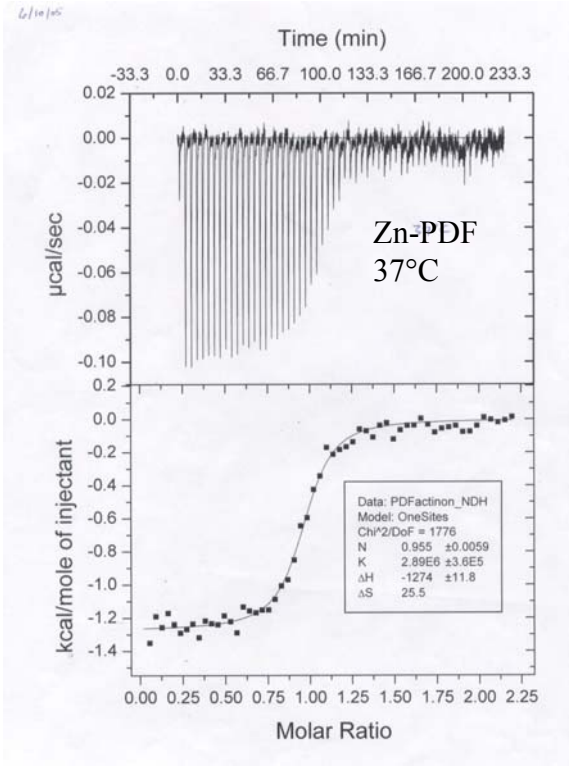
Time (min)
Zn-PDF
37°C
µcal/sec
kcal/mole of injectant
Molar Ratio
Data: PDFactinon_NDH
Model: OneSites
Chi^2/DoF = 1776
N 0.955 ±0.0059
K 2.89E6 ±3.6E5
ΔH -1274 ±11.8
ΔS 25.5

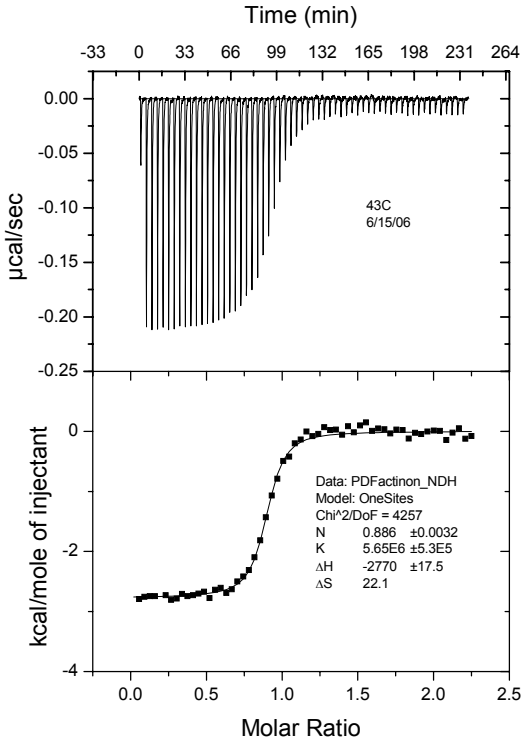

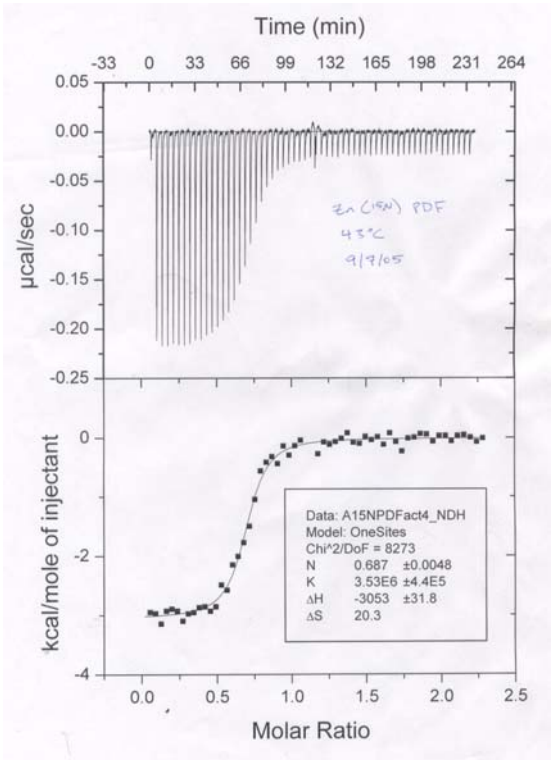

Different salt concentrations

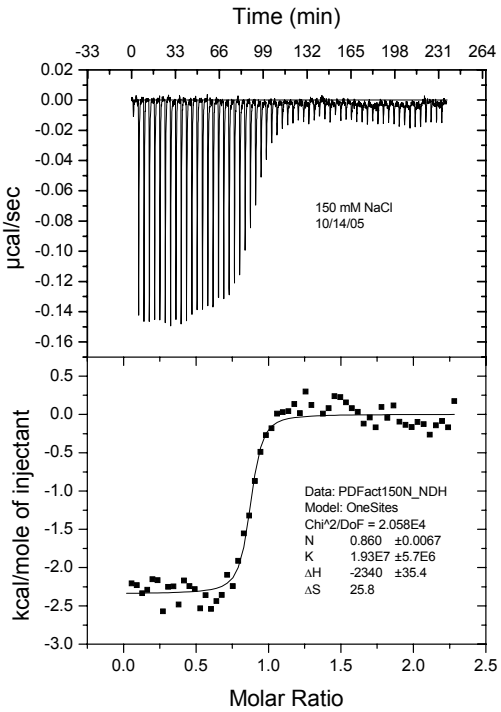

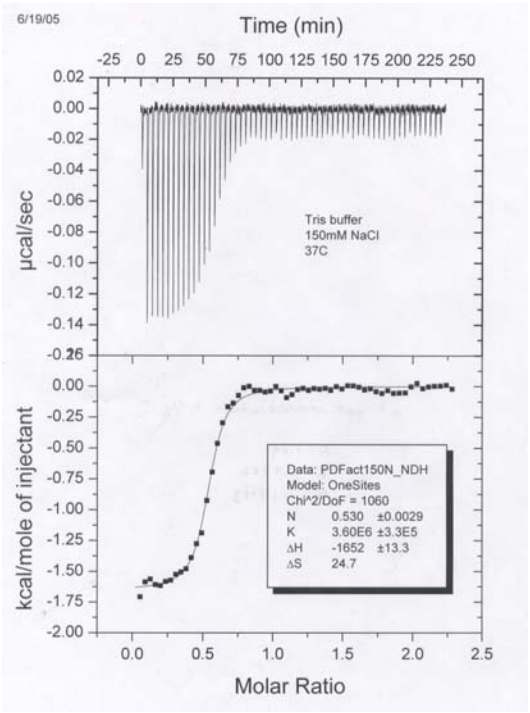

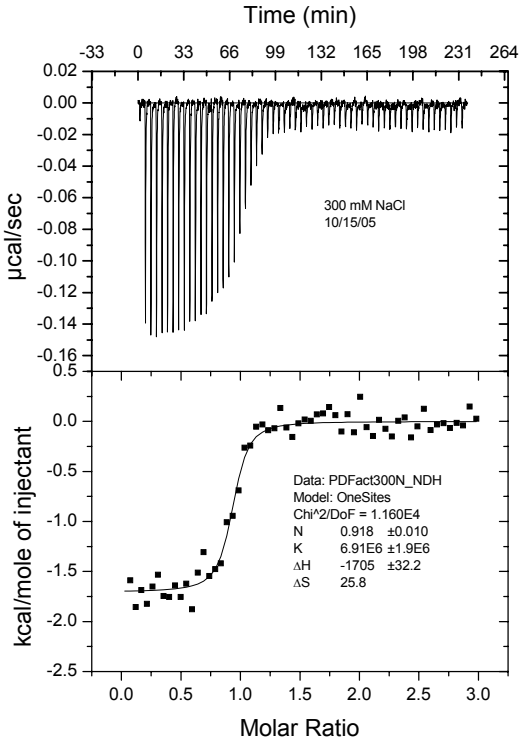
Time (min)
µcal/sec
300 mM NaCl
10/15/05
kcal/mole of injectant
Data: PDFact300N_NDH
Model: OneSites
Chi^2/DoF = 1.160E4
N 0.918 ±0.010
K 6.91E6 ±1.9E6
ΔH -1705 ±32.2
ΔS 25.8
Molar Ratio

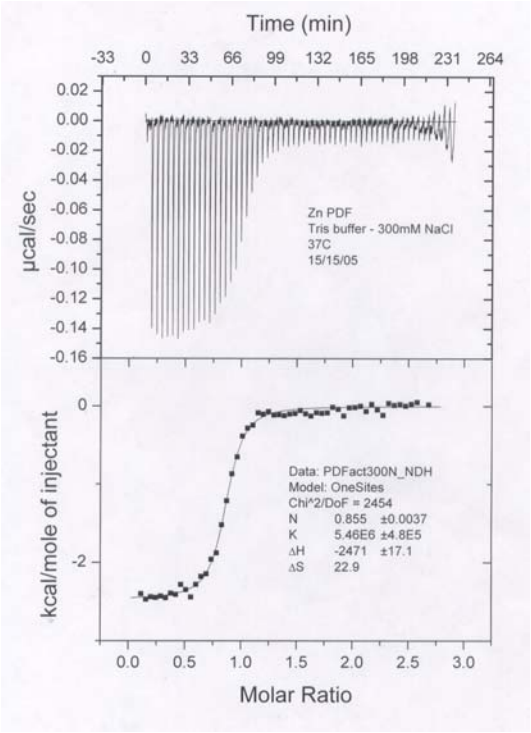
Time (min)
µcal/sec
Zn PDF
Tris buffer - 300mM NaCl
37C
15/15/05
kcal/mole of injectant
Data: PDFact300N_NDH
Model: OneSites
Chi^2/DoF = 2454
N 0.855 ±0.0037
K 5.46E6 ±4.8E5
ΔH -2471 ±17.1
ΔS 22.9
Molar Ratio

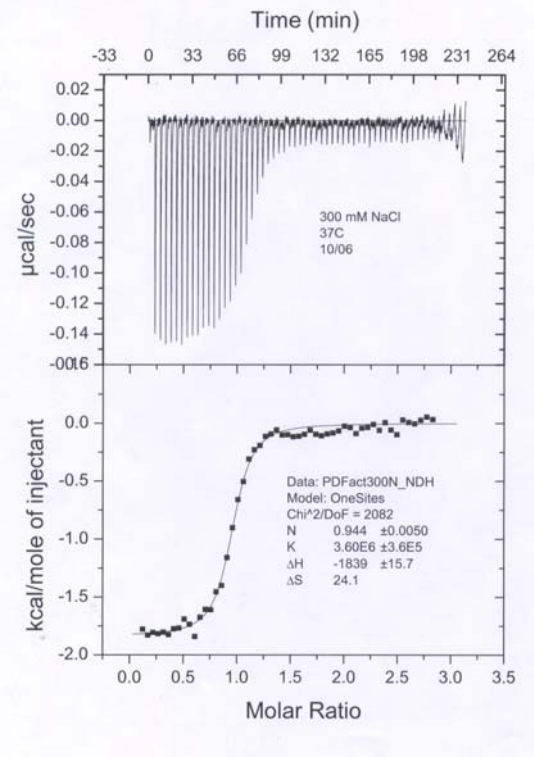
Time (min)
µcal/sec
300 mM NaCl
37C
10/06
kcal/mole of injectant
Data: PDFact300N_NDH
Model: OneSites
Chi^2/DoF = 2082
N 0.944 ±0.0050
K 3.60E6 ±3.6E5
ΔH -1839 ±15.7
ΔS 24.1
Molar Ratio

Different buffers

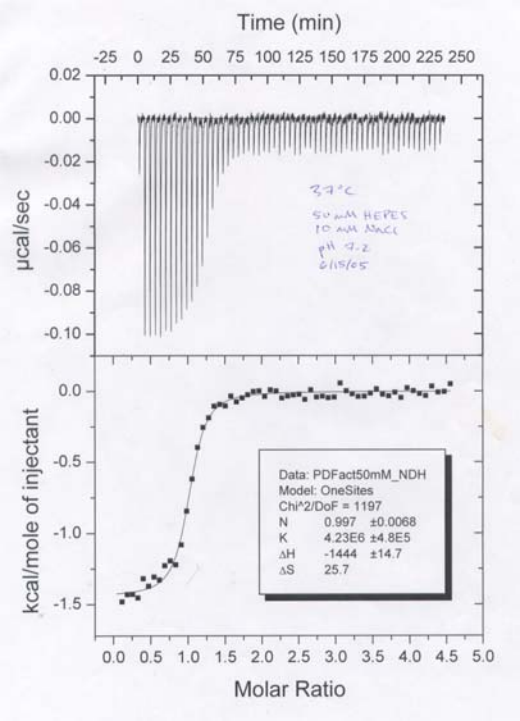

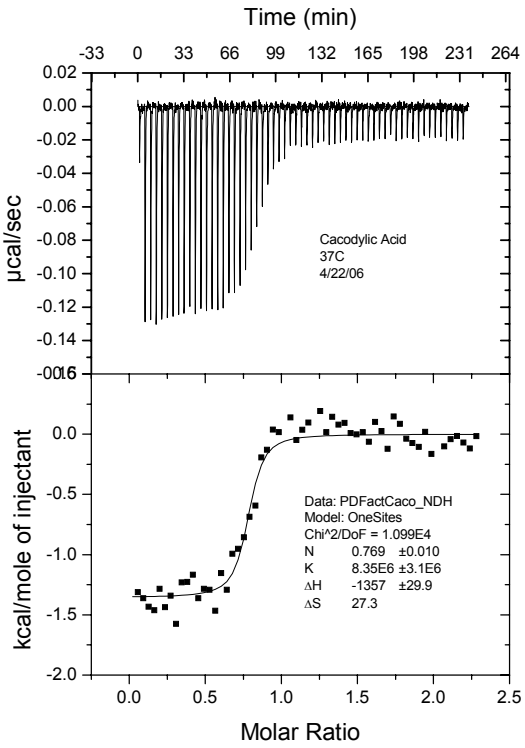

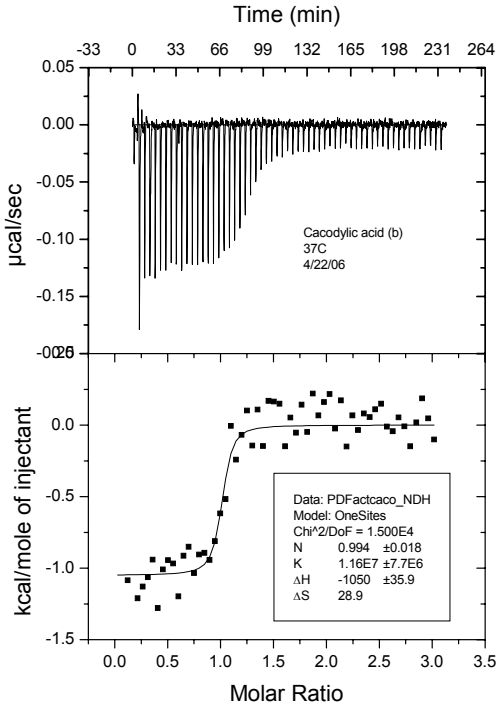

Different divalent cations

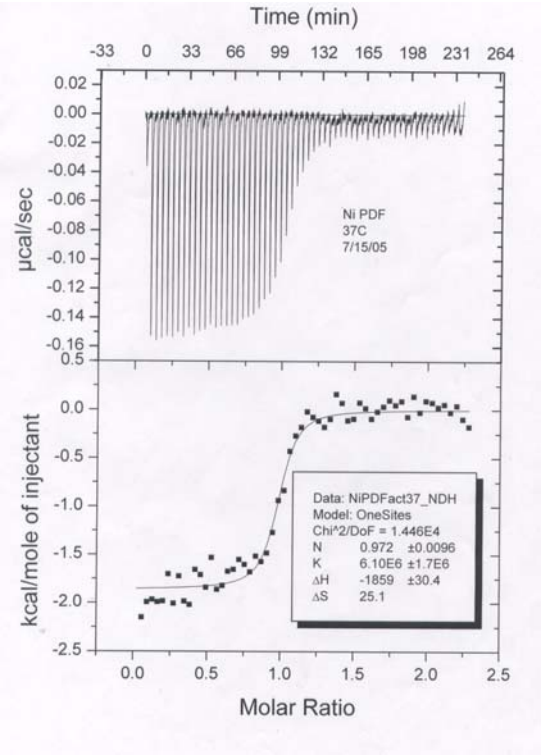

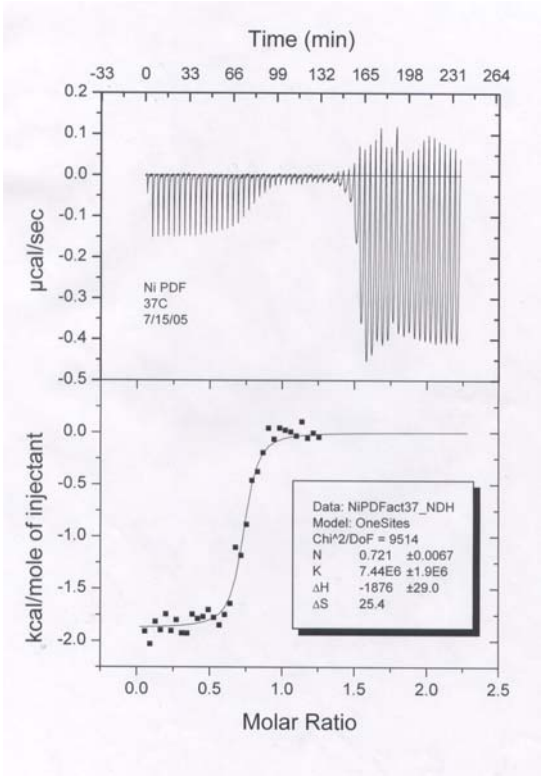

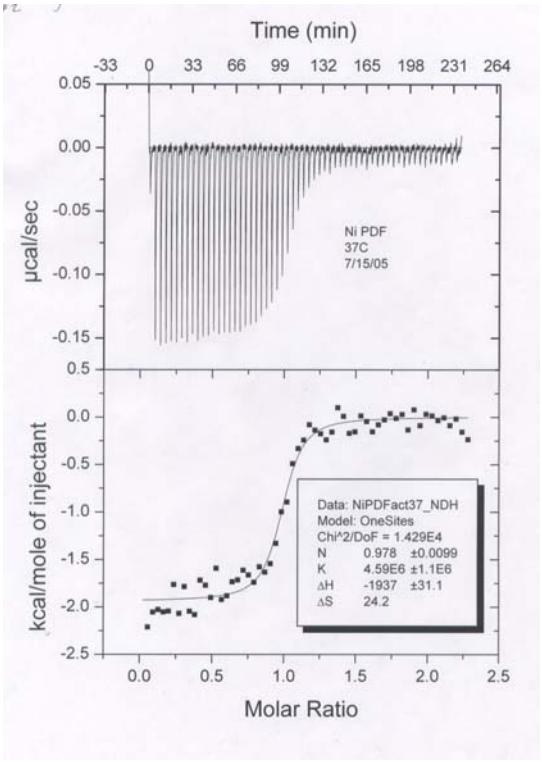

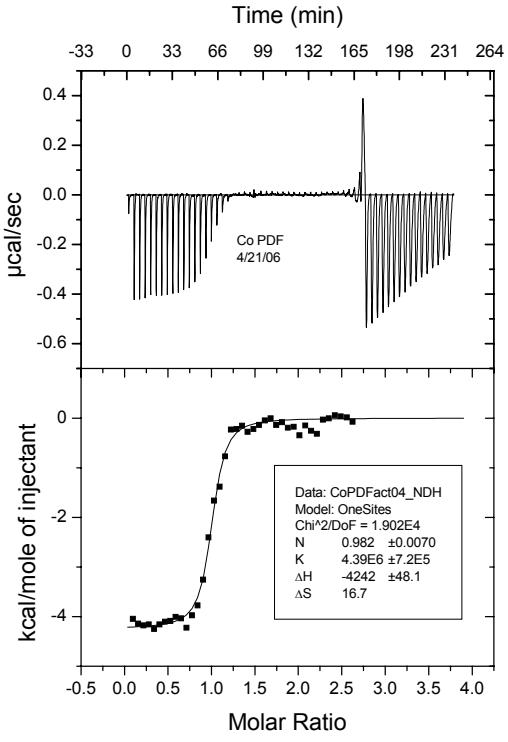

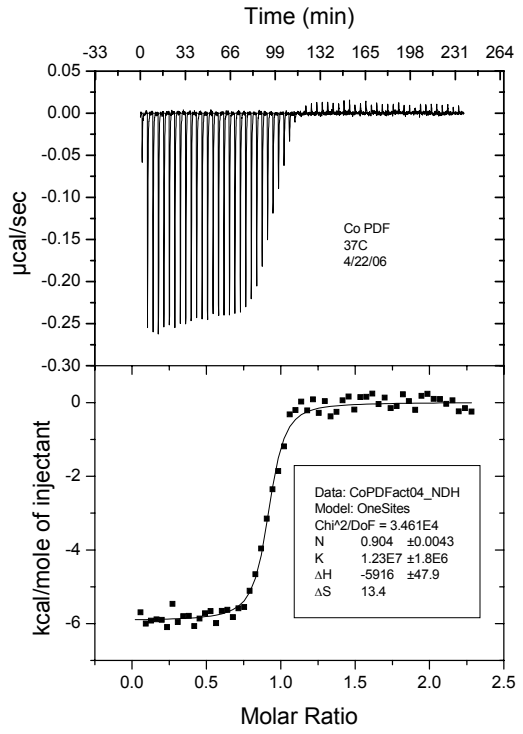
Time (min)
-33 0 33 66 99 132 165 198 231 264
µcal/sec
Co PDF
37C
4/22/06
kcal/mole of injectant
Data: CoPDFact04_NDH
Model: OneSites
Chi^2/DoF = 3.461E4
N 0.904 ±0.0043
K 1.23E7 ±1.8E6
ΔH -5916 ±47.9
ΔS 13.4
Molar Ratio

Summary of all ITC data

	Date	K_A (cal/mol)	Delta H (cal/molK)	Delta G (cal/molK)	-T*Delta S (cal/molK)
Metals					
Zinc					
37C	6/10/2005	2.89E+06	-1274	-9164	-7890
37C		1.36E+07	-1557	-10118	-8561
Average		8.25E+06	-1416	-9809	-8394
Cobalt					
Co	4/21/2006	4.39E+06	-4242	-9421	-5179
Co	4/22/2006	1.23E+07	-5916	-10056	-4140
Average		8.35E+06	-5079	-9817	-4738
Nickel					
Ni	7/15/2005	7.44E+06	-1876	-9746	-7870
Ni	7/15/2005	4.59E+06	-1937	-9449	-7512
Ni	7/15/2005	6.10E+06	-1859	-9624	-7765
Average		6.04E+06	-1891	-9618	-7727
Temperatures					
13C	6/14/2005	5.14E+06	2133	-9518	-11651
13C	9/7/2005	4.97E+06	3120	-9498	-12618
Average		5.06E+06	2627	-9508	-12135
19C	6/14/2005	5.46E+06	1423	-9556	-10979
37C	6/10/2005	2.89E+06	-1274	-9164	-7890
37C		1.36E+07	-1557	-10118	-8561
Average		8.25E+06	-1416	-9809	-8394
43C	6/15/2006	5.65E+06	-2770	-9577	-6807
43C	9/7/2005	3.53E+06	-3053	-9287	-6234
Average		4.59E+06	-2912	-9432	-6520
Buffers					
TRIS					
37C	6/10/2005	2.89E+06	-1274	-9164	-7890
37C		1.36E+07	-1557	-10118	-8561
Average		8.25E+06	-1416	-9809	-8394

	Date	KA	Delta H	Delta G	-T*Delta S
HEPES					
HEPES	6/15/2005	4.23E+06	-1444	-9398	-7954
Cacodylic acid					
Caco	4/22/2006	1.16E+07	-1050	-10020	-8970
Caco	4/22/2006	8.35E+06	-1357	-9817	-8460
Average		9.98E+06	-1204	-9927	-8723
Salt Concentrations					
10 mM					
37C	6/10/2005	2.89E+06	-1274	-9164	-7890
37C		1.36E+07	-1557	-10118	-8561
Average		8.25E+06	-1416	-9809	-8394
150 mM	10/14/2005	1.93E+07	-2340	-10333	-7993
150 mM	6/19/2005	3.60E+06	-1652	-9299	-7647
Average		1.15E+07	-1996	-10012	-8016
300 mM	15/15/2005	5.46E+06	-2471	-9556	-7085
300 mM	10/2006	3.60E+06	-1839	-9299	-7460
300 mM	10/15/2005	6.91E+06	-1705	-9701	-7996
Average		5.32E+06	-2005	-9540	-7535

References:

1. U. S. Food and Drug Administration, "Facts About Antibiotic Resistance," http://www.fda.gov/oc/opacom/hottopics/antiresist_facts.html

2. BBC News, "MRSA strain kills two in hospital," http://news.bbc.co.uk/1/hi/health/6188801.stm, Dec.18, 2006

3. Drobniewski F, Balabanova Y, Ruddy M, Weldon L, Jeltkova K, Brown T, et al. "Rifampin- and Multidrug-resistant tuberculosis in Russian civilians and prison inmates: dominance of the Beijing strain family," *Emerg Infect Dis* http://www.cdc.gov/ncidod/eid/vol8no11/02-0507.htm (2002)

4. Wawrik, Boris. "Bio-prospecting of uncultured microbes for novel antibiotics," http://aesop.rutgers.edu/~icbg/2005_training_course/wawrik_bioprospecting_of_microbes.pdf (2005)

5. Byerly, D.W. "Structure and Dynamics of Ligand Binding to E. coli Peptide Deformylase," Dissertation, The Ohio State University (2002)

6. Byerly, D.W., Amero, C., McElroy, C.A., Wilson, R.C., Foster, M.P. "Ligand-induced changes in the structure and dynamics of *E. coli* peptide deformylase" [*in preparation*]

7. Nguyen, Kiet T., "Mechanism, Function, and Inhibition of Peptide Deformylase," Dissertation The Ohio State University (2005)

8. Nguyen, K.T., Hu, X., Colton, C., Chakrabarti, R., Zhu, M.X., Pei, D "Characterization fo a Human Peptide Deformylase: Implications for Antibacterial Drug Design" *Biochemistry* **42**:9952-9958 (2003)

9. Leeds, Jennifer A., Dean, Charles R. "Peptide deformylase as an antibacterial target, a critical assessment," *Curr.Op.Pharm* **6**:445-452 (2006)

10. Meinnel, T., Lazennec, C. *et al.* "The C-terminal domain of peptide deformylase is disordered and dispensable for activity," *FEBS Lett* **385**(1-2):91-95 (1996)

11. Chan, M.K., Gong, W., Rajagopalan, P.T., Hao, B., Tsai, C.M., Pei, D. "Crystal structure of the Escherichia coli peptide deformylase," *Biochemistry* **36**:13904-13909 (1997)

12. Meinnel, T., Lazennec, C., *et. al*. "Mapping of the active site zinc ligands of peptide deformylase," *J.Mol.Biol.* **254**(2):175-183 (1995)

13. Chan, M.K., Gong, W., *et. al*. "Crystal structure of the *Escherichia coli* peptide deformylase," *Biochemistry* **36**(45):13904-13909 (1997)

14. Ragusa, S., Blanquet, S., Meinnel, T. "Control of Peptide Deformylase Activity by Metal Cations," *J.Mol.Biol.* **280**:515-523 (1998)

15. Chen, D.Z., Patel, D.V., Hackbarth, C.J, Wang, W., Dreyer, G., Young, D.C., Margolis, P.S., Wu, C., Ni, Z-J., Trias, J., White, R.J., Yuan, Z. "Actinonin, a naturally occurring antibacterial agent, is a potent deformylase inhibitor," *Antimicrob.Agents Chemother.* **45**(2):563-570 (2000)

16. Dardel, F., Ragusa, S., Lazennec, C., Blanquet, S., Meinnel, T. "Solution structure of nickel-peptide deformylase," *J.Mol.Biol.* **280**:501-513 (1998)

17. Meinnel, T., Blanquet, S., Dardel, F. "A new subclass of the zinc metalloproteases superfamily revealed by the solution structure of peptide deformylase," *J.Mol.Biol.* **262**:375-386 (1996)

18. Hao, B., Gong, W., Rajagopalan, P.T., Zhou, Y., Pei, D., Chan, M.K. "Structural basis for the design of antibiotics targeting peptide deformylase," *Biochemistry* **38**:4712-4719 (1999)

19. Guilloteau, J.P., Mathieu, M., Giglione, C., Blanc, V., Dupuy, A., Chevrier, M., Gil, P., Famechon, A., Meinnel, T., Mikol, V. "The crystal structures of four peptide deformylases bound to the antibiotic actinonin reveal two distinct types: a platform for the structure-based design of antibacterial agent,s" *J.Mol.Biol.* **320**:951-962 (2002)

20. Cai, J., Han, C., Hu, T., Zhang, J., Wu, D., Wang, F., Liu, Y., Ding, J., Chen, K., Yue, J., Shen, X., Jiang, H. "Peptide deformylase is a potential target for anti-Helicobacter pylori drugs: reverse docking, enzymatic assay, and X-ray crystallography validation," *Protein Sci.* **15**: 2071-2081 (2006)

21. Jain, R., Hao, B., Liu, R.-P., Chan, M.K. "Structures of E. coli peptide deformylase bound to formate: insight into the preference for Fe^{2+} over Zn^{2+} as the active site metal," *J.Am.Chem.Soc.* **127**:4558-4559 (2005)

22. Molteni, V., He, X., Nabakka, J., Yang, K., Kreusch, A., Gordon, P., Bursulaya, B., Warner, I., Shin, T., Biorac, T., Ryder, N.S., Goldberg, R., Doughty, J., He, Y. "Identification of novel potent bicyclic peptide deformylase inhibitors," *Bioorg.Med.Chem.Lett.* **14**:1477-1481 (2004)

23. Clements, J.M., Beckett, R.P., Brown, A., Catlin, G., Lobell, M., Palan, S., Thomas, W., Whittaker, M., Wood, S., Salama, S., Baker, P.J., Rodgers, H.F., Barynin, V., Rice, D.W., Hunter, M.G. "Antibiotic activity and characterization of BB-3497, a novel peptide deformylase inhibitor," *Antimicrob.Agents Chemother.* **45**:563-570 (2001)

24. Becker, A., Schlichting, I., Kabsch, W., Groche, D., Schultz, S., Wagner, A.F. "Iron center, substrate recognition and mechanism of peptide deformylase," *Nat.Struct.Biol.* **5**:1053-1058 (1998)

25. Yoon, H.-J., Kim, H.L., Lee, S.K., Kim, H.-W., Kim, H.-W., Lee, J.Y., Mikami, B., Suh, S.W. "Crystal structure of peptide deformylase from Staphylococcus aureus in complex with actinonin, a naturally occurring antibacterial agent," *Proteins* **57**:639-642 (2004)

26. Zhou, Z., Song, X., Gong, W. "Novel conformational states of peptide deformylase from pathogenic bacterium Leptospira interrogans: implications for population shift," *J.Biol.Chem.* **280**:42391-42396 (2005)

27. Becker, A., Schlichting, I., Kabsch, W., Schultz, S., Wagner, A.F. "Structure of peptide deformylase and identification of the substrate binding site," *J.Biol.Chem.* **273**:11413-11416 (1998)

28. Roques, B.P. "Cell surface metallopeptidases involved in blood pressure regulation: structure, inhibition, and clinical perspectives," *Pathol.Biol.* (Paris) **46**(3):191-200 (1998)

29. O'Brien, P.M., Ortwine, D.F., *et. al.* "Structure-activity relationships and pharmacokinetic analysis for a series of potent, systemically available biphenylsulfonamide matrix metalloproteinase inhibitors," *J.Med.Chem.* **43**(2):156-166 (2000)

30. Parkin, E.T., Trew, A., *et. al.* "Structure-activity relationship of hydroxamate-based inhibitors on the secretases that cleave the amyloid precursor protein, angiotensin converting enzyme, CD23, and pro-tumor necrosis factor-alpha," *Biochemistry* **41**(15):4972-4981 (2002)

31. Gordon, J.J., Kelly, B.K., Miller, G.A. "Actinonin: an Antibiotic Substance produced by an Actinomycete," *Nature* **195**:701-702 (1962)

32. Ramanathan-Girish, S., McColm, J., Clements, J.M., Taupin, P., Barrowcliffe, S., Hevizi, J., Safrin, S., Moore, C., Patou, G., Moser, H., Gadd, A., Hoch, U., Jiang, V., Lofland, D., Johnson, K.W. "Pharmacokinetics in Animals and Humans of a First-in-Class Peptide Deformylase Inhibitor" *Antimicrob Agents Chemother.* **48**(12) 4835-4842 (2004)

33. Clements, J.M., Beckett, R.P., Brown, A., Catlin, G., Lobell, M., Palan, S., Thomas, W., Whittaker, M., Wood., S., Salama, S., Baker, P.J., Rodgers, H.F., Barynin, V., Rice, D.W. "Antibiotic Activity and Characterization of BB-3497, a Novel Peptide Deformylase Inhibitor," *Antimicrob.Agents Chemother.* **45**(2):563-570 (2001)

34. Fritsche, T.R., Sader, H.S., Cleeland, R., Jones, R.N., "Comparative Antimicrobial Characterization of LBM415 (NVP PDF-713), a New Peptide Deformylase Inhibitor of Clinical Importance," *Antimicrob.Agents Chemother.* **49**(4):1468-1476 (2005)

35. Rajagopalan, P.T., Grimme, S., Pei, D. "Characterization of cobalt(II)-substituted peptide deformylase: function of the metal ion and the catalytic residue Glu-133," *Biochemistry* **39**(4):779-90 (2000)

36. Fersht, Alan. Structure and Mechanism in Protein Science. W. H. Freeman and Company: New York. (1998)

37. Tinoco, Ignacio, Jr., Sauer, K., Wang, J.C., Puglisi, J.D. Physical Chemistry Principles and Applications in Biological Sciences, 4th edition. Pretice Hill: Upper Saddle River, NJ (2002)

38. McElroy, C.A., Manfredo, A., Gollnick, P., Foster, M.P. "Thermodynamics of Tryptophan-Mediated Activation of the *trp*- RNA Binding Attenuation Protein" *Biochemistry* **45**:7844-7853 (2006)

39. Spolar, R.S., Record, M.T. Jr. "Coupling of Local Folding to Site-Specific Binding of Proteins to DNA," *Science* **263**:777-784 (1994)

40. Prabhu, N., Sharp, K. "Protein-Solvent Interactions" Chem. Rev. 106(5):1616-23 (2006)

41. Baker, B.M., Murphy, K.P. "Evaluation of Linked Protonation Effects in Protein Binding Reactions Using Isothermal Titration Calorimetry" *Biophys. J.* **71**:2049-2055 (1994)

42. Goldberg, R.N, Kishore, N., Lennen, R.M. "Thermodynamic Quantities for the Ionization Reactions of Buffers" *J. Phys. Chem. Ref. Data* **31**(2):231-370 (2002)

43. MicroCal, LLC *VP-ITC MicroCalorimeter User's Manual*, www.microcal.com

44. Spera, S., Ikura, M., Bax, A. "Measurement of the exchange rates of rapidly exchanging amide protons: application to the study of calmodulin and its complex with a myosin light chain kinase fragment," *J.Biomol.NMR* **1**(2):155-65 (1991)

45. Houry, W.A., Sauder, J. M., Roder, H, Scheraga, H. A. "Definition of amide protection factors for early kinetic intermediates in protein folding," *Proc. Natl. Acad. Sci.* **95** 4299-4302 (1998)